

## Mutual Passivation in Dilute GaN<sub>x</sub>As<sub>1-x</sub> Alloys

K. M. Yu<sup>1</sup>, W. Walukiewicz<sup>1</sup>, J. Wu<sup>2</sup>, D. E. Mars<sup>3</sup>, M. A. Scarpulla<sup>1,4</sup>, O. D. Dubon<sup>1,4</sup>, M. C. Ridgway<sup>5</sup>, and J. F. Geisz<sup>6</sup>

<sup>1</sup> Materials Sciences Division, Lawrence Berkeley National Laboratory, Berkeley, CA 94720

<sup>2</sup> Agilent Laboratories, 3500 Deer Creek Road, Palo Alto, CA 94304

<sup>3</sup> Dept. Chemistry and Chemical Biology, Harvard University, Cambridge, MA

<sup>4</sup> Department of Materials Science and Engineering, University of California, Berkeley, CA 94720

<sup>5</sup> Australian National University, Canberra, Australia

<sup>6</sup> National Renewable Energy Laboratory, Golden, Colorado 80401

### ABSTRACT

The dilute GaN<sub>x</sub>As<sub>1-x</sub> alloys (with x up to 0.05) have exhibited many unusual properties as compared to the conventional binary and ternary semiconductor alloys. We report on a new effect in the GaN<sub>x</sub>As<sub>1-x</sub> alloy system in which electrically active substitutional group IV donors and isoelectronic N atoms passivate each other's activity. This mutual passivation occurs in dilute GaN<sub>x</sub>As<sub>1-x</sub> doped with group IV donors through the formation of nearest neighbor IV<sub>Ga</sub>-N<sub>As</sub> pairs when the samples are annealed under conditions such that the diffusion length of the donors is greater than or equal to the average distance between donor and N atoms. The passivation of the shallow donors and the N<sub>As</sub> atoms is manifested in a drastic reduction in the free electron concentration and, simultaneously, an increase in the fundamental bandgap. This mutual passivation effect is demonstrated in both Si and Ge doped GaN<sub>x</sub>As<sub>1-x</sub> alloys. Analytical calculations of the passivation process based on Ga vacancies mediated diffusion show good agreement with the experimental results.

### INTRODUCTION

In recent years we witnessed the emergence of a new class of semiconductor alloys, the highly mismatched alloys (HMAs) which exhibit an unusually large band gap bowing. In these HMAs only a small amount of more electronegative elements (typically from less than 1% to several %) substituting the metallic anion of the III-V or II-VI matrix semiconductors results in large modification in the conduction band structure of the alloys. A most notable and well studied example is GaN<sub>x</sub>As<sub>1-x</sub>, in which strong band gap bowing by as much as 180 meV per mole percent of N (i.e. for x=0.01) has been observed [1-4]. Comparably large band gap reductions have also been observed in other III-N<sub>x</sub>-V<sub>1-x</sub> alloys such as GaInNAs, GaNP, InNP and AlGaNAs [4-9]. The strong dependence of the band gap on the N content has made these dilute III-V nitrides important materials for a variety of applications [10-13]. Theoretical and experimental aspects of the III-N-V alloys were extensively investigated and have been reviewed recently in a series of articles [14-17]. In close analogy, the formation of group II-O-VI HMAs by partial substitution of group VI anions with electronegative O in II-VI compounds has also been recently demonstrated [18].

Several theoretical studies have addressed the unusually strong dependence of the fundamental gap on the N content in the group III-N-V alloys [14-17]. The observation of an additional feature above the fundamental gap in the optical spectrum of GaInNAs alloys [19-21] as well as the unusual pressure dependence of these transitions led to the development of a band anticrossing model (BAC) [19,22] to explain the conduction band modification due to the presence of N in these alloys. In this BAC model, an anticrossing interaction between localized N-states and the extended states of the host semiconductor matrix splits the conduction band into two subbands. The downward shift of the lower subband is responsible for the reduction of the fundamental band gap and optical transitions from the valence band to the upper subband account for the high-energy edge. The model has been successfully used to quantitatively describe the dependencies of the upper and lower subband energies on hydrostatic pressure and on N content of  $\text{Ga}_{1-y}\text{In}_y\text{N}_x\text{As}_{1-x}$ ,  $\text{Ga}_{1-y}\text{Al}_y\text{N}_x\text{As}_{1-x}$ ,  $\text{InN}_x\text{P}_{1-x}$  and  $\text{GaN}_x\text{P}_{1-x}$  alloys [8, 19, 23-25].

In the BAC model, the dispersion relations for the upper and lower conduction subbands are given by:

$$E_{\pm}(k) = \frac{1}{2} \left[ E_N + E_M(k) \pm \sqrt{(E_N - E_M(k))^2 + 4C_{NM}^2 x} \right] \quad (1)$$

where  $E_N$  is the energy of the N level,  $E_M(k)$  is the dispersion relation for the host semiconductor matrix, and  $C_{NM}$  is the matrix element describing the coupling between N-states and the extended states. For  $\text{GaN}_x\text{As}_{1-x}$ , the downward shift of the lower subband  $E_-$  can account well for the reduction of the fundamental band gap using a value of  $E_N=1.65$  eV above the valence band maximum derived from PL measurements in N-doped GaAs [26] and  $C_{NM}=2.7$  eV from fitting the band gap variation data with N content [19,22]. A detail description of the BAC model can be found in reference 27.

This anticrossing interaction also leads to a considerable flattening of the lower subband near its minimum which in turn results in a large increase of the electron effective mass [21,28]. Recent reports have shown that the modified conduction band in  $\text{GaN}_x\text{As}_{1-x}$  enables a large enhancement in the maximum achievable free electron concentration  $n_{max}$  as compared to GaAs [29,30]. In a heavily Se-doped  $\text{Ga}_{1-3x}\text{In}_{3x}\text{N}_x\text{As}_{1-x}$  alloy thin film with only 3.3% of nitrogen, maximum free electron concentration  $n_{max}$  as high as  $7 \times 10^{19} \text{cm}^{-3}$  was achieved, more than one order of magnitude larger than that of GaAs [29].

In this paper we demonstrate the existence of an entirely new effect in  $\text{GaN}_x\text{As}_{1-x}$  in which an electrically active substitutional group donor and an isovalent N atom passivate each other's electronic effects [31-33]. We also derive the diffusion equation of Si donors taking into account both the Fermi-level independent (neutral vacancy mediated) and Fermi-level dependent (charged vacancy mediated) diffusion mechanisms. The resultant analytical equation shows good agreement with the measured electron concentration.

## EXPERIMENTAL DETAILS

$\text{GaN}_x\text{As}_{1-x}$  and  $\text{Ga}_{1-y}\text{In}_y\text{N}_x\text{As}_{1-x}$  thin films with thickness of  $\sim 0.5 \mu\text{m}$  were grown by molecular beam epitaxy (MBE) on semi-insulating GaAs substrates at substrate temperature of  $\sim 400^\circ\text{C}$ . In some cases, Indium was introduced to compensate the N-induced lattice contraction.

Si dopants were introduced during the growth. The epitaxially grown samples were rapid thermally annealed (RTA) in a flowing  $N_2$  ambient in the temperature range of 550-950°C for 10-120 s with the sample surface protected by a blank GaAs wafer.

The Ge doped  $GaN_xAs_{1-x}$  layers were synthesized by sequential implantation of Ge and N ions into GaAs followed by a combination of pulsed laser melting (PLM) and rapid thermal annealing (RTA) (PLM-RTA). Multiple energy  $Ge^+$  and  $N^+$  implantations were carried out into semi-insulating GaAs substrates forming a  $\sim 0.2\mu m$  thick layer with uniform distribution of N and Ge with  $\sim 2$  mole percent ( $\sim 4.4 \times 10^{20} cm^{-3}$ ) of both species (2%N+2%Ge). Layers produced from only N (2%N) or Ge (2%Ge) ion implantations were also used as references. The implanted GaAs samples were subjected to PLM in air using a KrF laser ( $\lambda = 248$  nm) with a FWHM pulse duration of  $\sim 38$  ns and fluence of  $0.45 J/cm^2$ . The samples were subsequently processed by RTA at temperatures between 600 and 950°C for 5-120 seconds in flowing  $N_2$ . We have recently utilized this method to realize  $GaN_xAs_{1-x}$  layers with  $x$  as high as 0.016 [34,35].

The free carrier concentration was measured by the Hall Effect technique in the Van der Pauw geometry. The band gaps of the films were measured using photomodulated reflectance (PR) at room temperature using a chopped HeCd laser beam ( $\lambda = 442$  nm or 325 nm) for modulation. Photoluminescence (PL) measurements were generated in the backscattering geometry by excitation with the 515 nm line of an argon laser.

## RESULTS AND DISCUSSION

### Maximum electron concentration enhancement in $GaN_xAs_{1-x}$

As we have mentioned earlier, the BAC model not only explains the band gap reduction in III-N<sub>x</sub>-V<sub>1-x</sub> alloys but it also predicts that the N-induced modifications of the conduction band may have profound effects on the transport properties of this material system [36]. In particular, the downward shift of the conduction band edge and the enhancement of the DOS effective mass in GaInNAs may lead to much enhanced maximum electron concentration  $n_{max}$ . Fig. 1 shows the electron concentration in Se doped MOCVD-grown  $Ga_{1-3x}In_{3x}N_xAs_{1-x}$  films with  $x=0$  to 0.033 measured by Hall Effect and electrochemical capacitance-voltage (ECV) technique [29]. Since the Se atomic concentrations in these films are at least an order of magnitude higher than the free electron concentration (in the range of  $2\sim 7 \times 10^{20} cm^{-3}$ ), the measured free electron concentration

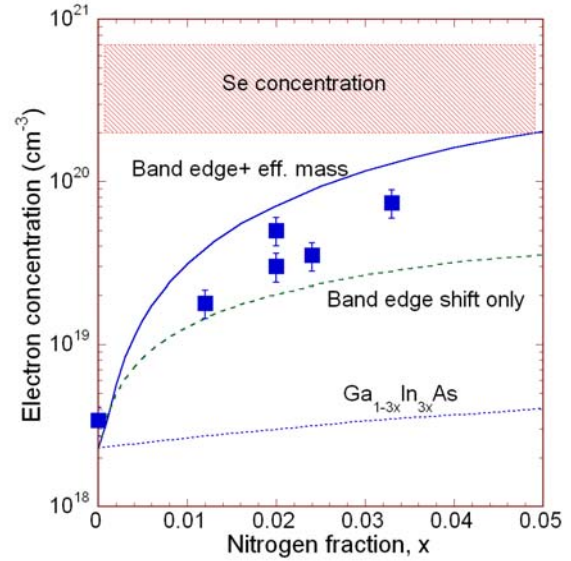


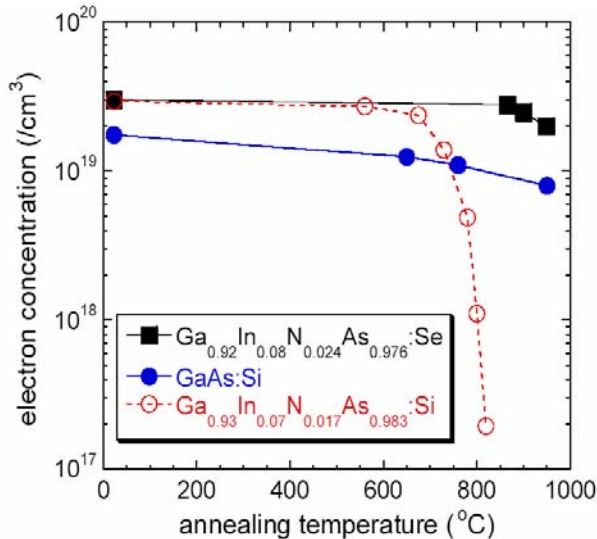
**Figure 1.** Comparison of the measured maximum electron concentration with the calculated values as a function of N fraction in  $Ga_{1-3x}In_{3x}N_xAs_{1-x}$ . Two different cases of the calculated  $n_{max}$  are shown (see text for details). The calculated  $n_{max}$  for samples with no N are also shown in the figure (dotted curve). The shaded area indicates the range of Se concentration in these

shown in Fig. 1 can be considered to be the maximum achievable free electron concentration,  $n_{\max}$ .

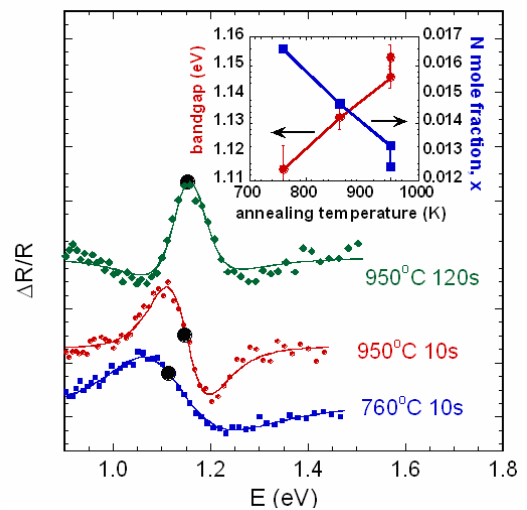
Fig. 1 shows that the  $n_{\max}$  increases strongly with the N content  $x$  with a maximum observed value of  $7 \times 10^{19} \text{ cm}^{-3}$  for  $x=0.033$ . This value is  $\sim 20$  times of that found in a GaAs film ( $3.5 \times 10^{18} \text{ cm}^{-3}$ ) grown under the same conditions. The much-enhanced  $n_{\max}$  in  $\text{Ga}_{1-3x}\text{In}_{3x}\text{N}_x\text{As}_{1-x}$  films can be explained by considering the N-induced conduction band modifications. According to the amphoteric native defect model the maximum free electron concentration is determined by the Fermi energy which is constant with respect to the Fermi stabilization energy  $E_{\text{FS}}$  [37]. Therefore the downward shift of the conduction band edge toward  $E_{\text{FS}}$  and the enhancement of the DOS effective mass in GaInNAs lead to much larger concentration of uncompensated, electrically active donors for the same location of the Fermi energy relative to  $E_{\text{FS}}$ . The calculated  $n_{\max}$  as a function of  $x$  for  $\text{Ga}_{1-3x}\text{In}_{3x}\text{N}_x\text{As}_{1-x}$  due to the downward shift of the conduction band caused by the level anticrossing only (dashed curve), as well as that including the increase in the effective mass (solid curve) are also shown in Fig. 1. Comparison of the experimental data with the calculation shows that in order to account for the large enhancement of the doping limits in III-N-V alloys both the effects of band gap reduction and the increase in the effective mass have to be taken into account.

### Mutual passivation of Si and N in MBE grown GaInNAs:Si

In contrast to the observed enhancement of the doping activation of the group VI elements (S, Se), Si and N co-implantation in GaAs only resulted in a highly resistive layer. This asymmetry in the behavior of group VI and IV donors can be explained by an entirely new effect in which an electrically active substitutional group IV donor and an isovalent N atom passivate each other's electronic effects [32]. This mutual passivation occurs in  $\text{GaN}_x\text{As}_{1-x}$  doped with group IV donors (Si and Ge) through the formation of nearest neighbor  $\text{IV}_{\text{Ga}}\text{-N}_{\text{As}}$  pairs.



**Figure 2.** Electron concentration of  $\text{In}_{0.07}\text{Ga}_{0.93}\text{As}_{0.983}\text{N}_{0.017}:\text{Si}$  is compared with those of GaAs:Si and Se doped  $\text{In}_{0.08}\text{Ga}_{0.92}\text{As}_{0.976}\text{N}_{0.024}$  as a function of annealing temperature for 10 s.



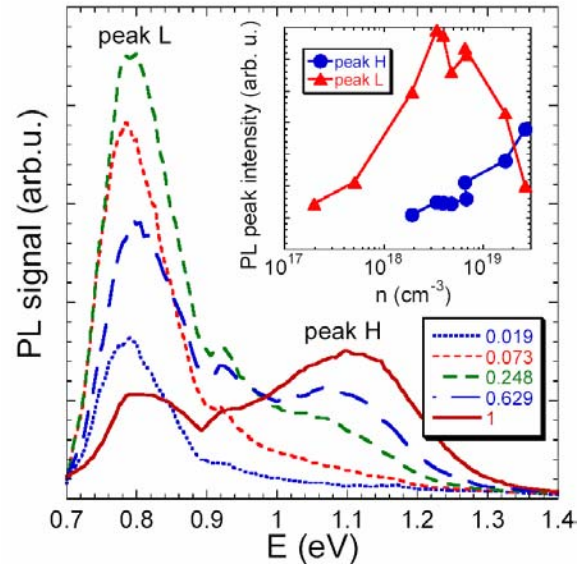
**Figure 3.** PR spectra of Si doped  $\text{In}_{0.07}\text{Ga}_{0.93}\text{As}_{0.983}\text{N}_{0.017}$  samples with different anneals. The inset shows the bandgap energies and active N mole fraction estimated from the BAC model as a function of annealing temperature.

Fig. 2 shows the free electron concentration in MBE-grown Si doped  $\text{Ga}_{0.93}\text{In}_{0.07}\text{N}_{0.017}\text{As}_{0.983}$  and GaAs as well as a MOCVD-grown Se doped  $\text{Ga}_{0.92}\text{In}_{0.08}\text{N}_{0.024}\text{As}_{0.976}$  thin films after RTA for 10 sec in the temperature range of 650-950°C. The Si and Se doping levels in these samples are in the range of  $2\text{-}9 \times 10^{19} \text{cm}^{-3}$  and  $\sim 2 \times 10^{20} \text{cm}^{-3}$ , respectively. For both the GaAs:Si and InGaAsN:Se samples, as the RTA temperature increases we observe only incremental decrease in electron concentrations, from  $1.6 \times 10^{19}$  to  $8 \times 10^{18} \text{cm}^{-3}$  for GaAs:Si and  $3 \times 10^{19}$  to  $2 \times 10^{19} \text{cm}^{-3}$  for InGaAsN:Se. Such a decrease in the electron concentration in GaAs is in agreement with the equilibrium maximum electron concentration (in the range of  $10^{18}\text{-}10^{19} \text{cm}^{-3}$ ) suggested by the amphoteric native defect model [37].

In striking contrast, the free electron concentration in the InGaAsN:Si sample drops from  $1.1 \times 10^{19} \text{cm}^{-3}$  in the as-grown film to  $3 \times 10^{17} \text{cm}^{-3}$  after RTA at 950°C for 10 s. In fact, RTA at 950°C for 120 s further reduces the electron concentration to  $< 10^{15} \text{cm}^{-3}$ . The reduced electrical activity of Si donors in  $\text{GaIn N}_x\text{As}_{1-x}$  alloys was attributed to the formation of nearest neighbor  $\text{Si}_{\text{Ga}}\text{-N}_{\text{As}}$  pairs. The highly electronegative N atom strongly binds the fourth valence electron of Si, preventing it from acting as a hydrogenic donor. This suggests that because of the localized nature of the N-states in  $\text{GaN}_x\text{As}_{1-x}$  the passivation is limited to group IV donors that occupy Ga sites. This is supported by the small change in electrical behavior observed in the InGaAsN:Se thin film in which both the N and Se reside in the As sublattice and therefore cannot form nearest neighbor passivating pairs.

Since the nitrogen is responsible for a massive modification of the electronic structure of  $\text{GaN}_x\text{As}_{1-x}$  alloys, the extent to which the formation of these pairs affects the role of N atoms in the alloys is investigated. Fig.3 shows the PR spectra of a  $\text{Ga}_{0.93}\text{In}_{0.07}\text{N}_{0.017}\text{As}_{0.983}$  sample doped with  $[\text{Si}] \sim 9 \times 10^{19} \text{cm}^{-3}$  after different annealing cycles. The bandgap values determined from fitting the PR spectra with the standard third-derivative functional form (black dots) together with the active nitrogen mole fraction calculated using the BAC model (Eq. (1)) are shown in the inset as a function of the annealing temperature. The bandgap energy increases with increasing annealing temperature. Assuming that the increase is solely attributed to the deactivation of N atoms, the concentration of the deactivated N is  $\sim 8 \times 10^{19} \text{cm}^{-3}$ , i.e., close to the initial total Si concentration in the as-grown sample. This is consistent with the picture that the formation of  $\text{Si}_{\text{Ga}}\text{-N}_{\text{As}}$  pairs is responsible for the mutual passivation of both species. It passivates the electrical activity of Si donors and deactivates N as the isovalent dopant.

The  $\text{Si}_{\text{Ga}}\text{-N}_{\text{As}}$  pair strongly binds the fourth valence electron of Si, transforming this hydrogenic donor into a deep localized center. In Fig. 4 we show the PL spectra from a series of Si-doped  $\text{In}_{0.07}\text{Ga}_{0.93}\text{As}_{0.983}\text{N}_{0.017}$  samples annealed at different temperatures. As the RTA temperature increases the electron concentration



**Figure 4.** PL spectra of several samples of  $\text{In}_{0.07}\text{Ga}_{0.93}\text{As}_{0.983}\text{N}_{0.017}:\text{Si}$  with different normalized free electron concentration as a result of different annealing conditions. The inset shows the intensity of the two PL peaks as a function of electron concentration.

decreases as indicated in Fig. 2. The electron concentration shown in the figure is normalized to the as-grown sample ( $n=3 \times 10^{19} \text{cm}^{-3}$ ). Two peaks are clearly observed in the spectra. The higher energy PL peak (peak H) at 1.1 eV corresponds to the band-to-band transitions. With reduced electron concentration, this peak gradually disappears, possibly due to increasing concentration of unknown non-radiative recombination defects generated by the high temperature annealing.

A deep-level related broad peak (peak L) is observed at an energy of about 0.8 eV. As shown in the inset of Fig. 4 the intensity of this peak exhibits a non-monotonic dependence on the electron concentration. The maximum peak intensity occurs near  $n \sim 5 \times 10^{18} \text{cm}^{-3}$ . This also corresponds approximately to the concentration where the mobility reaches its maximum. We tentatively attribute peak L to optical transitions involving states associated with the the  $\text{Si}_{\text{Ga}}\text{-N}_{\text{As}}$  pairs. As the concentration of  $\text{Si}_{\text{Ga}}\text{-N}_{\text{As}}$  pairs increases with decreasing  $n$ , the emission intensity is enhanced. Upon further annealing, non-radiative transitions start to dominate the recombination process; as a result the intensities of both peak H and peak L vanish gradually.

### **Passivation via Ga vacancies mediated diffusion**

The microscopic nature of the passivation process was explored by considering the diffusion of substitutional Si atoms in GaInNAs alloys. We note that the diffusion coefficient  $D(T,t)$  of  $\text{Si}_{\text{Ga}}$  in GaAs can be expressed as a combination of the Fermi-level independent term (mainly via neutral Ga vacancies  $\text{V}_{\text{Ga}}^0$ )  $D^0(T)$  and the Fermi-level dependent term (via triply negatively charged Ga vacancies  $\text{V}_{\text{Ga}}^{3-}$ )  $D^{\alpha-}(T)[n(t)/n_i]$  [38,39]. Here  $\alpha = 3$  is the negative charge state of  $\text{V}_{\text{Ga}}^{3-}$ , and  $n_i$  is the intrinsic carrier concentration.

We assume  $D(T,t)$  is a slowly varying function that can be treated as a constant within a short period of time  $dt$ . According to the mutual passivation mechanism, the reduction rate of  $\text{Si}_{\text{Ga}}$  (hence of the free electron concentration  $n$ ) is proportional to the total number of active nitrogen atoms residing in the diffusion volume,

$$\frac{dn(t)}{n(t)} = -x \cdot dL(t) \propto x \cdot \frac{D(T,t)}{a^2} dt, \quad (2)$$

where  $a$  is the distance between nearest neighbors on the Ga sublattice, and  $x$  is the mole fraction of active N atoms. Since  $[\text{N}] \gg [\text{Si}]$  in our samples, we neglect the passivation of N caused by the Si-N pair formation, and replace  $x$  in Eq.(2) by the initial N fraction ( $x_0$ ). The solution of Eq. (2) is

$$\ln \left[ \frac{n(t)}{n_0} \right] = -\frac{1}{\alpha} \ln \left\{ \left( 1 + \frac{1}{r(T)} \right) \cdot \exp \left[ \frac{\alpha \beta x_0 D^0(T)}{a^2} \cdot t \right] - \frac{1}{r(T)} \right\}, \quad (3)$$

where  $\beta$  is a constant that is proportional to the Si passivation rate and  $r$  is the ratio of the  $\text{V}_{\text{Ga}}^0$  mediated and the  $\text{V}_{\text{Ga}}^{3-}$  mediated diffusion coefficients,

$$r(T) = \frac{D_0^0}{D_0^{\alpha-}} \cdot \exp \left[ -\frac{E_a^0 - E_a^{\alpha-}}{k_B T} \right] \cdot \left[ \frac{n_i}{n_0} \right]^\alpha.$$

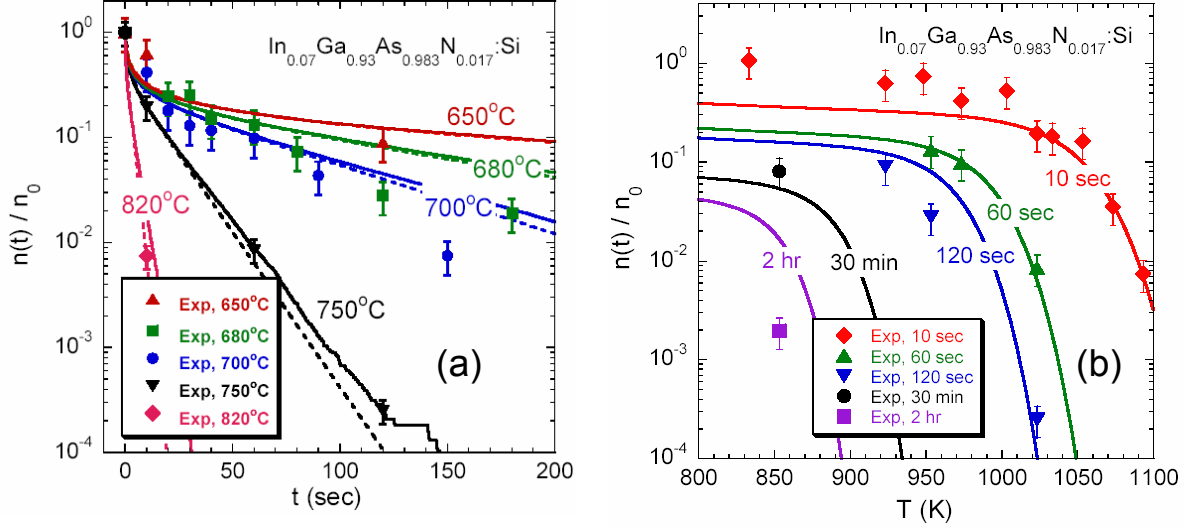


**Figure 5.** Normalized free electron concentration (log scale) as a function of (a) annealing time at different annealing temperatures and (b) annealing temperature with different annealing time. The solid and dashed curves represent the results from the analytical calculation (Eq.(2)).

Notice in Eq. (3) that  $\ln[n(t)/n_0]$  is linear in  $t$  for the cases of high temperature annealing ( $t \gg 1$ ) as well as long annealing time [32]. For both cases the reduction rate of  $n(t)$  is dominated by the Si diffusion facilitated by  $V_{\text{Ga}}^0$ .

Figures 5 (a) and (b) show the effect of isothermal and isochronal annealing on the free carrier concentration of the  $\text{Ga}_{0.93}\text{In}_{0.07}\text{As}_{0.983}\text{Si}$  sample with  $[\text{Si}] \sim 9 \times 10^{19} \text{ cm}^{-3}$  for annealing temperatures in the range 650-820°C. The curves represent calculations based on Eq.(3). It is evident that calculations are in good agreement with experiment. According to the diffusion model, at high annealing temperatures or long annealing time, the Fermi-level independent,  $V_{\text{Ga}}^0$ -mediated diffusion becomes increasingly important. This is reflected in the linear time dependence of the  $\ln[n/n_0]$  curves at high temperatures or long annealing durations.

It is important to note that, as shown in Fig. 5(b) the electron concentration starts to decrease rapidly for 10 s isochronal annealing, at  $\sim 700^\circ\text{C}$ . This threshold temperature roughly corresponds to the annealing conditions that allow the Si atoms to diffuse over a distance equal to the average separation between randomly distributed Si and N atoms ( $\sim 7\text{\AA}$ ). As expected, increasing the annealing time reduces the threshold temperature. With increasing annealing time, this onset shifts to lower temperatures. With 2 hr furnace annealing at temperatures as low as  $580^\circ\text{C}$ , more than two decades of drop in  $n$  was observed.

### Electronic transport properties

The precise control of the electron concentration over a wide range by mutual passivation provides a unique tool to investigate the concentration dependence of the electron mobility in III-N-V alloys with the same N content. It has been widely recognized that the incorporation of small amounts of nitrogen into GaAs leads to a drastic reduction of the electron mobility. The typical mobility of  $\text{GaN}_x\text{As}_{1-x}$  films ranges from  $\sim 10$  to a few hundred  $\text{cm}^2/\text{Vs}$  [4,40], which is over an order of magnitude smaller than the electron mobility in GaAs at comparable doping

levels [41]. Figure 6 shows the change in room-temperature mobility of  $\text{Ga}_{0.93}\text{In}_{0.07}\text{N}_{0.017}\text{As}_{0.983}:\text{Si}$  when the electron concentration is reduced by the formation of  $\text{Si}_{\text{Ga}}\text{-N}_{\text{As}}$  pairs. The mobility shows a non-monotonic dependence on the electron concentration with a maximum at  $n \sim 5 \times 10^{18} \text{cm}^{-3}$ .

By using the Green's function method within coherent potential approximation, we have shown that the two-level BAC model can be derived from the Hamiltonian of the many-impurity Anderson model that considers the hybridization of extended states and dilute localized states [27]. The imaginary part of the Green's function represents the broadening of the electronic states and can be used to determine the width of optical transitions and to calculate the free electron mobility. The broadening of the  $E_-$  subband  $\Gamma_-(\mathbf{k})$  defines a finite lifetime for the wavefunction of the restructured states  $|E_-(\mathbf{k})\rangle$  through the uncertainty principle, which imposes a limit to the mobility of free electrons in the lowest conduction band:

$$\mu_1 = \frac{e\tau(k_F)}{m_-^*(\mathbf{k}_F)} \approx \frac{e\hbar}{m_-^*(\mathbf{k}_F) \cdot \Gamma_-(\mathbf{k}_F)}. \quad (4)$$

In this equation, the electron effective mass at the Fermi surface ( $m_-^*(\mathbf{k}_F)$ ) can be calculated from the curvature of the dispersion  $E_-(\mathbf{k})$  [42]. The Fermi wavevector ( $\mathbf{k}_F$ ) and Fermi energy ( $E_F$ ) are determined by the free electron concentration calculated from the density of states of  $E_-(\mathbf{k})$  [27].

The room-temperature mobility ( $\mu_1$ ) calculated from Eq.(4) is shown as dotted curve. Also shown is the Fermi energy as a function of  $n$ . It is seen that at high electron concentrations when the Fermi energy approaches the original energy level of N localized states in  $\text{Ga}_{0.93}\text{In}_{0.07}\text{N}_{0.017}\text{As}_{0.983}$  (located at  $\sim 0.30$  eV above the conduction band edge of  $E^C$ , or 0.54 eV above the conduction band edge of  $E_-$ ), the mobility is largely suppressed by the strong hybridization between N localized states and the extended states of the matrix. At  $n = 2 \times 10^{19} \text{cm}^{-3}$ , the energy broadening and scattering lifetime at the Fermi surface are estimated to be 0.25 eV and 3 fs, respectively. The mean free path of free electrons is about 5 Å, which is only a third of the average distance between the randomly distributed N atoms. Therefore, at this electron concentration the homogeneous broadening resulting from the anticrossing interaction is the dominant scattering mechanism that limits the

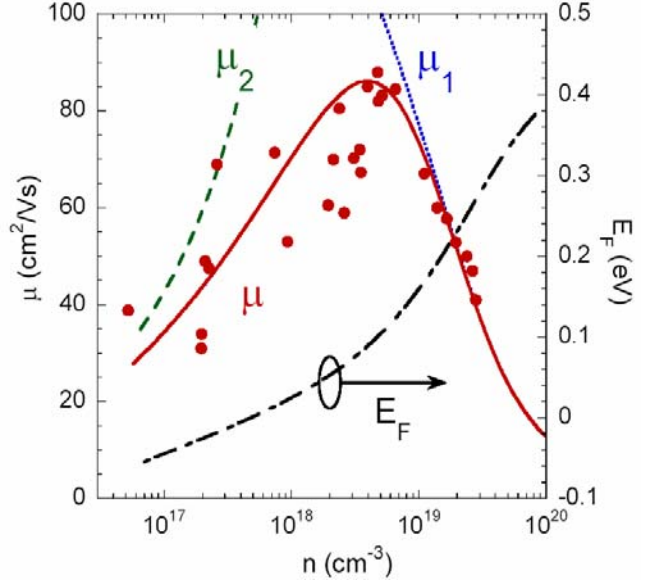


**Figure 6.** Room-temperature electron mobility of  $\text{In}_{0.07}\text{Ga}_{0.93}\text{As}_{0.983}\text{N}_{0.017}:\text{Si}$  plotted as a function of electron concentration. The calculated mobilities limited by the conduction band broadening ( $\mu_2$ ) and by the random field scattering ( $\mu_1$ ) are shown. The calculated Fermi energy is referenced to the bottom of the lowest conduction band ( $E_-$ ).

electron mobility. The fact that at high concentrations the electron mobility calculated from the BAC model is in a very good agreement with experiment without any adjustable parameters provides further support for the BAC description of the electronic structure of GaInNAs alloys.

Fig. 6 also shows that as the Fermi level moves down away from the original N level with decreasing electron concentration, the mobility continuously increases until  $E_F$  drops down to  $\sim 0.1$  eV corresponding to an electron concentration of about  $4.5 \times 10^{18} \text{ cm}^{-3}$ . At lower electron concentrations the mobility starts to decrease, deviating severely from the prediction of Eq.(6). This effect can be attributed to the scattering of the conduction electrons by the random fields caused by the structural and compositional disorder in the alloy [43,44].

An estimate for the electron mobility limited by the random field scattering ( $\mu_2$ ) is also shown in Fig. 6. A reasonable agreement with experiment is obtained with a random field distribution with 30 meV potential depth and 3 meV/Å potential gradient. Assuming that the potential fluctuations are solely caused by the inhomogeneity of the nitrogen distribution in  $\text{Ga}_{1-y}\text{In}_y\text{N}_x\text{As}_{1-x}$ , this potential depth corresponds to approximately a  $\sim 18\%$  change in  $x$  (*i.e.*,  $x = 0.017 \pm 0.003$ ). The solid curve in Fig. 6 takes into account the contributions of both the level broadening and random alloy scattering effects that limit the mobility ( $\mu = 1/(\mu_1^{-1} + \mu_2^{-1})$ ). This calculated mobility reproduces the non-monotonic behavior of the mobility measured over two decades of change in electron concentration.

### **Mutual passivation of Ge in GaNAs**

Finally, we confirm the general nature of the mutual passivation effect by investigations of  $\text{GaN}_x\text{As}_{1-x}$  layers doped with Ge, another group IV donor. Ge doped  $\text{GaN}_x\text{As}_{1-x}$  layers were synthesized by sequential implantation of Ge and N ions into GaAs followed by a combination of pulsed laser melting (PLM) and rapid thermal annealing (RTA). PLM was carried out using a KrF laser ( $\lambda = 248 \text{ nm}$ ) with pulse duration  $\sim 38 \text{ ns}$  and fluence of  $0.45 \text{ J/cm}^2$ . We have recently utilized this (PLM-RTA) method to realize  $\text{GaN}_x\text{As}_{1-x}$  layers with  $x$  as high as 0.016 [34,35].

The passivation of the N activity by the Ge atoms is illustrated in the series of PR spectra presented in Fig. 7. The band gap energies obtained from the PR spectra are shown in the inset as a function of the duration of 950°C RTA treatment. A fundamental band gap transition at 1.24 eV is observed for GaAs samples implanted with 2% N alone after PLM-RTA at 950°C for 10-120 s, corresponding to a  $\text{GaN}_x\text{As}_{1-x}$  layer with  $x \sim 0.01$ . In contrast, the band gap

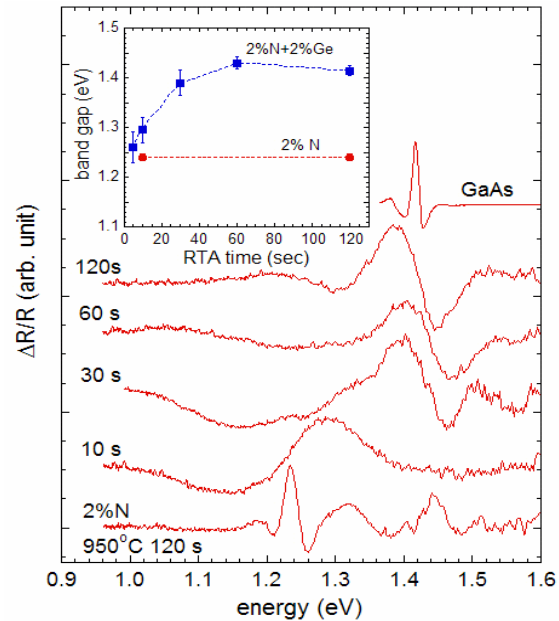


**Figure 7.** PR spectra from GaAs samples implanted with 2%N+2%Ge followed by PLM-RTA at 950°C for a duration of 5-120 s. PR spectra from a GaAs wafer (top spectrum) and a GaAs sample implanted with 2%N only after PLM+RTA at 950°C for 120 s. (bottom spectrum) are also shown. The inset shows the band gap energies of the samples after PLM+RTA at 950°C for durations of 5-120 s.

of the 2%N+2%Ge samples after PLM increases from 1.24 to 1.42 eV (band gap of GaAs) as the RTA duration increases to 60s, revealing that all  $N_{As}$  sites are passivated by Ge. The gradual increase in the band gap of the 2%N+2%Ge sample as a function of RTA temperature and/or time duration can be attributed to the passivation of  $N_{As}$  by  $Ge_{Ga}$  through the formation of nearest neighbor  $Ge_{Ga}-N_{As}$  pairs.

Fig. 8 shows a comparison of the electron concentration of the 2%N+2%Ge and 2%Ge samples followed by PLM-RTA for 10s in the temperature range of 650 to 950°C. The electron concentration of both samples approaches  $10^{19} \text{cm}^{-3}$  after PLM. This high electron concentration exceeding the equilibrium  $n_{max}$  results from the highly non-equilibrium rapid melting and solidification in the PLM process. For the 2%Ge sample, thermal annealing after PLM drives the system toward equilibrium with an electron concentration of  $\sim 1 \times 10^{18} \text{cm}^{-3}$  which is consistent with the amphoteric nature of Ge in GaAs [45]. The electron concentration of the 2%N+2%Ge samples, on the other hand, drops over two orders of magnitude to less than  $10^{17} \text{cm}^{-3}$  as the samples are subjected to RTA at temperatures higher than 650°C. The changes in the band gap and the electrical behavior in the Ge doped  $GaN_xAs_{1-x}$  sample show that the activities of Ge donors and isovalent N mutually passivate each other via the formation of  $N_{As}-Ge_{Ga}$  pairs, just as was the case in Si doped  $GaN_xAs_{1-x}$ .

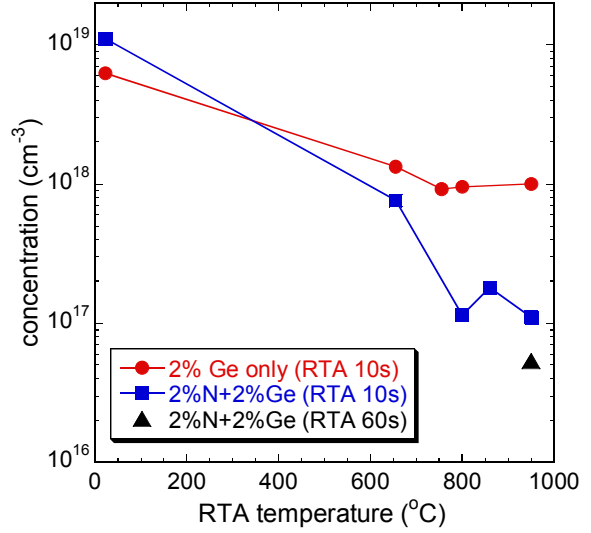


**Figure 8.** Free electron concentrations of the 2%Ge and 2%N+2%Ge samples after PLM+RTA at increasing temperature for 10 s. obtained by Hall effect measurements.

## CONCLUSIONS

We have demonstrated the mutual passivation phenomenon in highly mismatched  $GaN_xAs_{1-x}$  and  $Ga_{1-y}In_yN_xAs_{1-x}$  alloys doped with group IV shallow donors: Si and Ge. It is shown that upon thermal annealing, Si (Ge) donors diffuse in the Ga sublattice until forming  $Si_{Ga}-N_{As}$  ( $Ge_{Ga}-N_{As}$ ) nearest-neighbor pairs. This process results in the mutual passivation of electronic activities of Si (Ge) as a shallow donor and N as an isovalent impurity. The diffusion-passivation process is analyzed in the context of Si diffusion mediated by Ga vacancies. The free electron mobility has been measured and explained on the basis of the electron state broadening caused by the band anticrossing interaction between the N localized states and extended states of the host GaInAs. Moreover, the ability to use PLM for a spatially controlled passivation provides a unique opportunity for the fabrication of novel planar and three-dimensional structures by the selective implantation of either one or both species. The mutual passivation effect described here may therefore be exploited for electrical isolation, band gap engineering, and quantum confinement.

## ACKNOWLEDGEMENTS

We thank J. Beeman for ion implantation and Hartmut Bracht for helpful discussions. This work was supported by the Director, Office of Science, Office of Basic Energy Sciences, Division of Materials Sciences and Engineering, of the U. S. Department of Energy under Contract No. DE-AC03-76SF00098.

## REFERENCES

1. S. Sakai, Y. Ueta and Y. Terauchi, *Jpn. J. Appl. Phys.* **32**, 4413 (1993).
2. M. Kondow, K. Uomi, K. Hosomi, and T. Mozume, *Jpn. J. Appl. Phys.* **33**, L1056 (1994).
3. K. Uesugi, N. Morooka, and I. Suemune, *Appl. Phys. Lett.* **74**, 1254(1999).
4. J. F. Geisz, D. J. Friedman, J. M. Olson, S. R. Kurtz, and B. M. Keyes, *J. Cryst. Growth* **195**, 401 (1998).
5. J. N. Baillargeon, K. Y. Cheng, G. E. Hofler, P. J. Pearch and K. C. Hsieh, *Appl. Phys. Lett.* **60**, 2540 (1992).
6. W. Shan, W. Walukiewicz, K. M. Yu, J. Wu, J. W. Ager, E. E. Haller, H. P. Xin, and C. W. Tu, *Appl. Phys. Lett.* **76**, 3251 (2000).
7. W. G. Bi and C. W. Tu, *J. Appl. Phys.* **80**, 1934 (1996).
8. W. Shan, W. Walukiewicz, K. M. Yu, J. W. Ager III, E. E. Haller, J. F. Geisz, D. J. Friedman, J. M. Olson, Sarah R. Kurtz, and K. Nauka, *Phys. Rev.* **B62**, 4211 (2000).
9. W. Shan, K. M. Yu, W. Walukiewicz, J. W. Ager, E. E. Haller and M. C. Ridgway, *Appl. Phys. Lett.* **75**, 1410 (1999).
10. M. Kondow, T. Kitatani, S. Nakatsuka, M. C. Larson, K. Nakahara, Y. Yazawa, M. Okai and K. Uomi, *IEEE J. Sel. Topics in Quantum Elect.* **3**, 719 (1997).
11. M. Kondow, T. Kitatani, M. C. Larson, K. Nakahara, K. Uomi and H. Inoue, *J. Crystal Growth* **188**, 255 (1998).
12. D. J. Friedman, J. F. Geisz, S. R. Kurtz, D. Myers and J. M. Olson, *J. Cryst. Growth* **195**, 409(1998).
13. S. R. Kurtz, A.A. Allerman, E.D. Jones, J.M. Gee, J.J. Banas, and B.E. Hammons, *Appl. Phys. Lett.* **74**, 729(1999).
14. Special issue of Semicond. Sci Technol:*III-N-V Semiconductor Alloys* **17**, 741-906. (2002).
15. Special Issue of J. Physics:Condensed Matter:*Dilute Nitrides* **16 (31)**, S2295-3412 (2004).
16. Irina Buyanova and Weimin Chen ed., Physics and Applications of Dilute Nitrides, (Taylor & Francis, New York, 2004).
17. M. Henini, ed., Dilute Nitride Semiconductors, (Elsevier, Oxford, UK, 2005).
18. K. M. Yu, W. Walukiewicz, J. Wu, W. Shan, and J. W. Beeman, M. A. Scarpulla, O. D. Dubon, and P. Becla, *Phys. Rev. Lett.* **91**, 246203 (2003).
19. W. Shan, W. Walukiewicz, J. W. Ager III, E. E. Haller, J. F. Geisz, D. J. Friedman, J. M. Olson, and S. R. Kurtz, *Phys. Rev. Lett.* **82**, 1221(1999).
20. J. D. Perkins, A. Mascaranhas, Y. Zhang, J. F. Geisz, D. J. Friedman, J. M. Olson, and S. R. Kurtz, *Phys. Rev. Lett.* **82**, 3312 (1999).
21. P. Perlin, P. Wisniewski, C. Skierbiszewski, T. Suski, E. Kaminska, S. G. Subramanya, E. R. Weber, D. E. Mars, and W. Walukiewicz, *Appl. Phys. Lett.* **76**, 1279 (2000).

22. W. Walukiewicz, W. Shan, K. M. Yu, J. W. Ager III, E. E. Haller, I. Miotkowski, M. J. Seong, H. Alawadhi, A. K. Ramdas, *Phys. Rev. Lett.* 2000; **85**: 1552.
23. W. Shan, W. Walukiewicz, J. W. Ager III, E. E. Haller, J. F. Geisz, D. J. Friedman, J. M. Olson, and Sarah R. Kurtz, *J. Appl. Phys.* **86**, 2349(1999).
24. W. Shan, W. Walukiewicz, K. M. Yu, J. W. Ager III, E. E. Haller, H. P. Xin, and C. W. Tu, *Appl. Phys. Lett.* **76**, 3251 (2000).
25. K. M. Yu, W. Walukiewicz, W. Shan, J. Wu, J. W. Beeman, J. W. Ager III, E. E. Haller, H. P. Xin, and C. W. Tu, *Appl. Phys. Lett.* **78**, 1077 (2001).
26. D. J. Wolford, J. A. Bradley, K. Fry, and J. Thompson, in *Proceedings of the 17<sup>th</sup> International Conference on the Physics of Semiconductors*, edited by J. D. Chadi and W. A. Harrison (Springer, New York, 1984) p. 627.
27. J. Wu, W. Shan and W. Walukiewicz, *Semiconi. Sci. Tech.*, **17**, 860 (2002).
28. C. Skierbiszewski, P. Perlin, P. Wiśniewski, W. Knap, T. Suski, W. Walukiewicz, W. Shan, K. M. Yu, J.W. Ager, E.E. Haller, J.F. Geisz, and J.M. Olson, *Appl. Phys. Lett.* **76**, 2409 (2000).
29. K. M. Yu, W. Walukiewicz, W. Shan, J. W. Ager III, J. Wu, E. E. Haller, J. F. Geisz, D. J. Friedman, J. M. Olson, and Sarah R. Kurtz, *Phys. Rev. B* **61**, R13337 (2000).
30. K. M. Yu, W. Walukiewicz, W. Shan, J. Wu, J. W. Ager III, E. E. Haller, J. F. Geisz, and M. C. Ridgway, *Appl. Phys. Lett.* **77**, 2858 (2000).
31. K. M. Yu, W. Walukiewicz, J. Wu, D. Mars, D. R Chamberlin M. A. Scarpulla, O. D. Dubon, and J. F. Geisz, , *Nature Materials* **1**, 185 (2002).
32. J. Wu, K. M. Yu, W. Walukiewicz, G. He, E. E. Haller, D. E. Mars, D. R Chamberlin, *Phys. Rev. B* **68**, 195202 (2003).
33. K. M. Yu, W. Walukiewicz, J. Wu, W. Shan, J. Beeman, M. A. Scarpulla, O. D. Dubon, M. C. Ridgway, D. E. Mars, and D. R Chamberlin, *Appl. Phys. Lett.* **83**, 2844 (2003).
34. K. M. Yu, W. Walukiewicz, J. W. Beeman, M. A. Scarpulla, O. Dubon, M. R. Pillai, and M. Aziz, ” *Appl. Phys. Lett.* **80**, 3958 (2002).
35. K. M. Yu, W. Walukiewicz, M. A. Scarpulla, O. D. Dubon, J. Jasinski, Z. Liliental-Weber, J. Wu, J. W. Beeman, M. R. Pillai, and M. J. Aziz, *J. Appl. Phys.* **94**, 1043 (2003)
36. W. Walukiewicz, W. Shan, J. W. Ager III, D. R. Chamberlin, E. E. Haller, J. F. Geisz, D. J. Friedman, J. M. Olson, and S. R. Kurtz., *Proc. 195<sup>th</sup> Mtg. Electrochem. Soc.* 1999; Vol.**99-11**: 190-200.
37. W. Walukiewicz, *Physica B*, **302-303**, 123 (2001).
38. S. Yu, U. M. Goesele and T. Y. Tan, *J. Appl. Phys.* **66**, 2952 (1989).
39. T. Ahlgren, J. Likonen, J. Slotte, J. Ræisaenen, M. Rajatora and J. Keinonen, *Phys. Rev.* **B56**, 4597(1997).
40. Steven R. Kurtz, A. A. Allerman, C. H. Seager, R. M. Sieg, and E. D. Jones, *Appl. Phys. Lett.* **77**, 400 (2000).
41. J. S. Blakemore, *J. Appl. Phys.* **53**, R123 (1982).
42. C. Skierbiszewski, P. Perlin, P. Wisniewski, T. Suski, J. F. Geisz, K. Hingerl, W. Jantsch, D. E. Mars and W. Walukiewicz, *Phys. Rev.* **B65**, 035207 (2001).
43. V. L. Bonch-Bruevich, *phys. stat. sol.* **42**, 35 (1970).
44. P. G. Zhumatii, *phys. stat. sol. (b)* **75**, 61 (1976).
45. Y. K. Yeo, J. E. Ehret, F. L. Pedrotti, Y. S. Park, and W. M. Theis, *Appl. Phys. Lett.* **35**, 197 (1979).